AGU PUBLICATIONS

Geochemistry, Geophysics, Geosystems

TECHNICAL REPORTS: DATA

10.1002/2017GC007217

**Key Point:**
- Online database of geochronologic and geochemical data for the Himalayan-Tibetan orogeny

**Correspondence to:**
J. B. Chapman,
jaychapman@email.arizona.edu

**Citation:**
Chapman, J. B., & Kapp, P. (2017). Tibetan magmatism database. *Geochemistry, Geophysics, Geosystems*, *18*. https://doi.org/10.1002/2017GC007217

Received 1 SEP 2017
Accepted 27 SEP 2017
Accepted article online 29 SEP 2017



# Tibetan Magmatism Database

**James B. Chapman[1] and Paul Kapp[1]**

[1]Department of Geosciences, University of Arizona, Tucson, AZ, USA

**Abstract** A database containing previously published geochronologic, geochemical, and isotopic data on Mesozoic to Quaternary igneous rocks in the Himalayan-Tibetan orogenic system are presented. The database is intended to serve as a repository for new and existing igneous rock data and is publicly accessible through a web-based platform that includes an interactive map and data table interface with search, filtering, and download options. To illustrate the utility of the database, the age, location, and $\varepsilon Hf_t$ composition of magmatism from the central Gangdese batholith in the southern Lhasa terrane are compared. The data identify three high-flux events, which peak at 93, 50, and 15 Ma. They are characterized by inboard arc migration and a temporal and spatial shift to more evolved isotopic compositions.

**Plain Language Summary** A new database with a web-based interface is presented that contains compiled geochronologic, geochemical, and isotopic data on igneous rocks in the Himalaya-Tibetan orogen.

## 1. Introduction

The Himalayan-Tibetan orogenic system is the archetype for Cenozoic to present continental collision, the development of large orogenic plateaus, and for collision-related ore deposits (Yin & Harrison, 2000). When combined with other geologic information, the age, composition, and trace element and isotope geochemistry of igneous rocks from the Himalayan orogen and Tibetan Plateau provide insight into the tectonics and geodynamics of India-Asia collision (Yin, 2006, 2010). Classic tectonic problems/processes that rely upon the igneous rock record in the India-Asia collision include: (1) convective removal of the continental mantle lithosphere (Platt & England, 1994; Turner et al., 1993, 1996), (2) subduction of Indian continental lower crust and mantle lithosphere (DeCelles et al., 2002; Ding et al., 2003; Owens & Zandt, 1997; Powell, 1986), (3) intracontinental subduction of continental lithosphere (Arnaud et al., 1992; Deng, 1989; Roger et al., 2000; Tapponnier et al., 2001; Wang et al., 2001), (4) oceanic slab roll-back during closure of the Neo-Tethys ocean (Yin et al., 1994), (5) oceanic slab break-off following continental collision (Lee et al., 2009; Xu et al., 2008; Yin & Harrison, 2000), (6) crustal anataxis (Chung et al., 2003; Hou et al., 2012; Wang et al., 2005), (7) gravitational collapse (Burchfiel & Royden, 1985; Dewey et al., 1988; Harrison et al., 1992; Kapp & Guynn, 2004), and (8) lower crustal flow (Grujic et al., 2002; Lee & Whitehouse, 2007; Royden et al., 1997), among many others.

This database is an effort to centralize Tibetan geochronologic, geochemical, and isotopic data for the Earth science community and has grown out of numerous ad hoc databases that we and others have created to examine specific phenomena or processes (e.g., Chapman et al., 2017; Chung et al., 2009; DeCelles et al., 2011; Yin, 2010; Zhu et al., 2011). Data from the Himalayan orogen and Tibetan Plateau have proliferated rapidly since the advent of LA-ICP-MS zircon U-Pb and zircon Lu-Hf isotopic analyses. The database is inspired by other widely utilized igneous rock databases that focus on a specific area or orogenic system, including the North American volcanic and intrusive rock database (NAVDAT; http://www.navdat.org) and the Central Andes geochemical GPS database (Mamani et al., 2010; http://andes.gzg.geo.uni-goettingen.de), both of which examine Mesozoic to recent magmatism.

## 2. Database

The data are contained in a Google Sheets™ web-based spreadsheet that is read by a web application, Awesome Table (https://awesome-table.com), where the data are reformatted and organized, before being

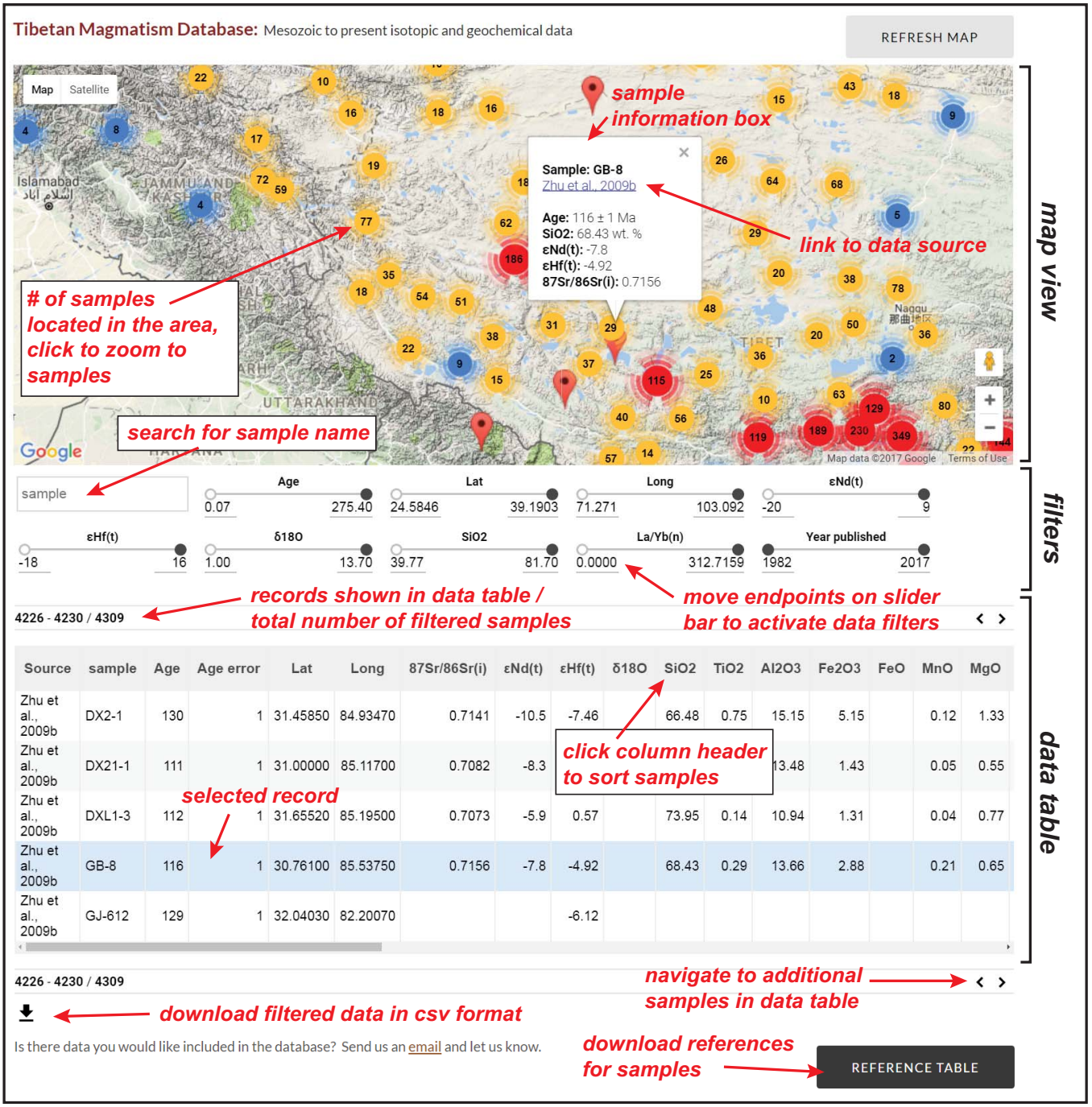


**Figure 1.** Screenshot of the online interface for the Tibetan magmatism database. Major features and functions are labeled.

embedded into a host website. Online access to the Tibetan magmatism database is currently available at http://www.jaychapman.org/tibet-magmatism-database.html and is optimized for most major internet browsers. The layout of the online interface contains an interactive data table, map, and a series of filters (Figure 1).

The map view is linked to Google Maps™ and has the same features as Google Maps™, including road, terrain, and satellite imagery basemaps. Upon loading, the map view shows several circles of different colors (Figure 1). The number in each circle is the number of samples in the region covered by that circle. By zooming in or selecting a circle, the samples within that area appear. Selecting a sample location will bring

up an information box in map view and highlight the sample information in the data table (Figure 1). Included in the information box is a reference with a hyperlink to the online data source, usually a journal article.

Below the map view is a search bar for sample names and a series of filters that can be manipulated by clicking and dragging the endpoints (Figure 1). Clicking the left endpoint once is equivalent with a "not null" filter and will bring up all samples that contain the type of data specific to that filter. For example, clicking once on the left endpoint on the "Age" filter will load all samples with age information. Changes to the filters are reflected in the map view and data table. The number of samples that meet the filter criteria is shown at the top left and bottom left of the data table (Figure 1).

The data table displays up to five samples at a time and additional samples can be viewed by clicking the left or right arrows at the top right or bottom right of the data table (Figure 1). Data can be ordered in ascending or descending values by selecting a column header. Selecting a sample in the data table brings up the location and information box for that sample in the map view. Filtered data can be downloaded as a comma-separated values (csv) file by selecting the down arrow at the bottom left of the data table (Figure 1).

## 3. Data

All samples are igneous rocks and data come from sources that have been peer-reviewed. Unpublished data are excluded. A table of references to the original data source is available in Microsoft Excel™ format by selecting the "Reference Table" button at the bottom right of the website (Figure 1). In general, samples with no geographic location information are excluded. In cases where sample locations were only presented on a map in the data source, the map was georeferenced and sample locations estimated. Locations are recorded in decimal degree format (°N latitude and °E longitude) using the WGS 84 reference coordinate system.

Sample ages are crystallization ages (in Ma) and based on the mean or "interpreted" age reported in the data source. Age uncertainties are reported as provided in the data source and are not always provided at the $2\sigma$ level. Age data come from a variety of geochronologic methods, but are mainly zircon U-Pb data. Commonly, many samples are geochemically analyzed from a single location or igneous body, but only a few samples are dated. In these cases, an approximate age is assigned to each sample; however, no age uncertainty is assigned in the database. Only Mesozoic and Cenozoic samples are presently included in the database.

Major elements are reported in wt % and trace elements are reported in ppm. Where applicable, trace element normalization values are from McDonough and Sun (1995). All radiogenic isotope ratios are reported at the time of crystallization. Lu-Hf and Sm-Nd isotopic data are reported using epsilon notation. For normalization, $\varepsilon Nd_t$ and $\varepsilon Hf_t$ values are reported using present-day $^{143}Nd/^{144}Nd_{CHUR} = 0.512638$ and $^{176}Hf/^{177}Hf_{CHUR} = 0.28286$ (Faure & Mensing, 2005). $^{87}Sr/^{86}Sr_i$ and $\varepsilon Nd_t$ are whole rock values and are reported as presented in the data source. $\varepsilon Hf_t$ and $\delta^{18}O$ (in ‰) are commonly measured in zircon extracted from the rock sample. $\delta^{18}O$ values may include whole rock and mineral analyses other than zircon (e.g., quartz) and may involve differing normalization schemes. $\delta^{18}O$ data are presented chiefly to help quickly identify studies that analyzed oxygen isotopes in any material. Some $\varepsilon Hf_t$ values are from whole rock analyses, however, there is only minor Hf isotope fractionation between zircon and the parent whole rock (Kinny & Maas, 2003). "Interpreted" $\delta^{18}O$ and $\varepsilon Hf_t$ values are reported if presented in the data source, otherwise an unweighted mean from multiple single analyses (e.g., zircon analyses) is reported.

Data coverage is uneven and influenced by sampling bias. For example, the region surrounding Lhasa (city) represents ~15% of the total data set. Near Lhasa, and in other places, data were preferentially generated from regions with recognized ore deposits. Other regions, such as the northern and northeastern Tibetan Plateau, are under sampled. The majority of data from the Himalaya are associated with leucogranite in the Greater Himalayan sequence and northern Himalayan gneiss domes (Yin, 2006).

## 4. Example Application

To demonstrate the scientific usefulness of the database, samples from the central (85°E–95°E longitude) Gangdese batholith in the southern Lhasa terrane are plotted (Figure 2). The data identify three high-flux events (HFE) that peak at 93, 50, and 15 Ma, consistent with previous data compilations from the Gangdese

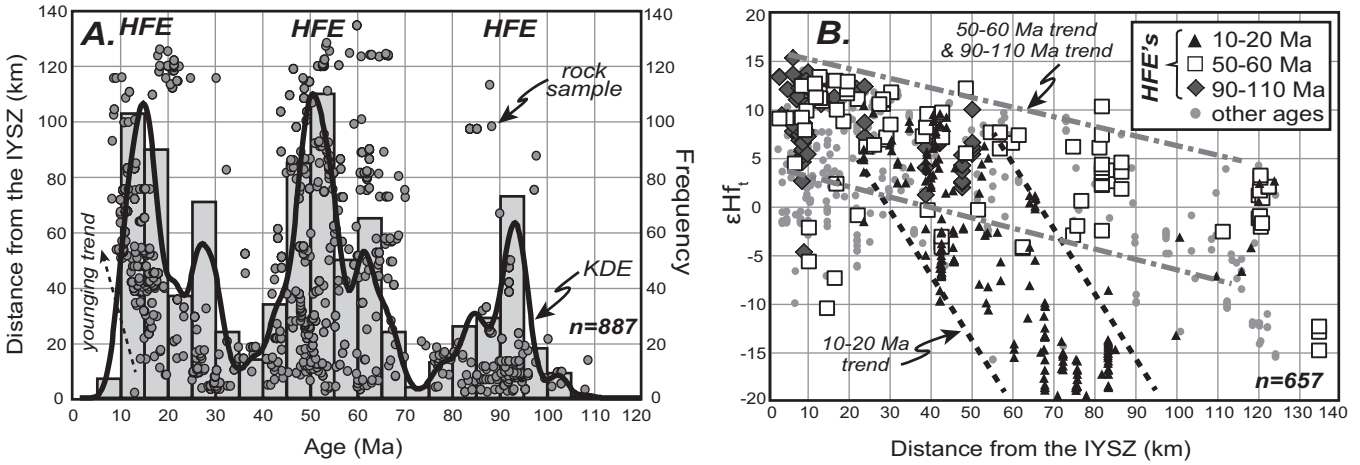


**Figure 2.** (a) Mid-Cretaceous and younger igneous rock ages (circles; uncertainties not shown for clarity) from the central Gangdese batholith plotted against sample location, shown as distance ~North of the Indus-Yarlung suture zone (IYSZ), measured perpendicular to the trend of the suture zone. Also shown is a histogram and kernel density estimate (KDE) for the age of the samples. Figure 2a shows that the location of magmatism broadened or migrated inboard (North) during major flare-up or high-flux events (HFE). There is also a prominent northward younging trend of magmatism between 20 and 8 Ma. (b) A subset of data from Figure 2a that have $\varepsilon Nd_t$ or $\varepsilon Hf_t$ isotopic information available (uncertainties not shown for clarity) plotted against sample location. Both whole rock $\varepsilon Nd_t$ and zircon $\varepsilon Hf_t$ data are shown, with $\varepsilon Nd_t$ converted to $\varepsilon Hf_t$ using the terrestrial array of Vervoort et al. (1999). Spatial isotopic trends are labeled by HFE.

arc (Ji et al., 2009; Zhu et al., 2011). Although periodic HFE are present in almost all magmatic arcs, the primary mechanisms responsible for HFE are still debated (Ducea et al., 2015). The 93 Ma event precedes India-Asia collision and has been attributed to ridge subduction or roll-back of the Neo-Tethyan oceanic slab (Kapp et al., 2007; Zhang et al., 2010). The 50 Ma event has been attributed to break-off of the subducted Neo-Tethyan oceanic slab after initial India-Asia collision (Yin & Harrison, 2000; Zhu et al., 2011). The 15 Ma event has been attributed to delamination of Asian mantle lithosphere concomitant with and perhaps accelerated by underthrusting of Indian lithosphere (Chung et al., 2009; Sundell et al., 2013).

Each HFE is characterized by broadening or inboard migration of magmatism (Figure 2a). The inboard migration of magmatism is also associated with an inboard decrease in $\varepsilon Hf_t$ (Figure 2b), which has been interpreted to reflect a spatial change from asthenospheric to lithospheric mantle melt source regions (Chapman et al., 2017). HFE are commonly associated with temporal isotopic "pull-downs" to more evolved compositions (DeCelles et al., 2009). The data from the Gangdese arc suggests that these pull-downs may also be associated with arc migration (Figure 2b).

The northward younging trend of $<$20 Ma magmatism in the Gangdese batholith and complete shut-off of the Gangdese arc by ~8 Ma (dashed arrow; Figure 2a) is consistent with underthrusting of Indian lithosphere following break off of Indian continental lithosphere in the early Miocene (Chemenda et al., 2000; DeCelles et al., 2011; Replumaz et al., 2010). The 10–20 Ma trend in Figure 2b indicates a more isotopically evolved source north of the Indus-Yarlung suture zone compared to magmatism $>$50 Ma. The 10–20 Ma trend may be related a greater component of lower crustal melting, metasomatization of the Asian mantle lithosphere by melting/devolatilization of the underthrust Indian lithosphere (Ding et al., 2003), and/or southward viscous entrainment of isotopically evolved Northern Lhasa terrane mantle lithosphere with the subducting Indian plate (Kelly et al., 2016).

## 5. Conclusions

Geochronologic, geochemical, and isotopic data on Mesozoic to recent igneous rocks from the Himalayan-Tibetan orogen and the Tibetan Plateau region are compiled in a web-based database. An online interface to easily explore, filter, and download the data contained in the database has been created and made publically accessible. Magmatic rock data are particularly powerful in the aggregate, and the database is anticipated to help generate and test hypotheses. Data from the Gangdese batholith in the southern Lhasa terrane were compiled as an example of how the database may be utilized. The compilation identifies three HFE (93, 50, and 15 Ma) that occur before, during, and after initial India-Asia collision. Despite the varied

tectonic environments, each HFE is characterized by northward migration of magmatism and more evolved isotopic compositions of magmatism located farther north from the Indus-Yarlung suture zone. The 15 Ma HFE is characterized by a northward younging trend and a more isotopically evolved melt source region in the northern Gangdese batholith that may be related to underthrusting of Indian lithosphere and delamination or convective removal of Asian continental lithosphere.

**Acknowledgments**
Development of the Tibetan magmatism database was part of the data dissemination plan for a project funded by National Science Foundation grant EAR-1008527 (P.K.). The database can be accessed at www.jaychapman.org/tibet-magmatism-database.html. Reviews by An Yin and two anonymous reviewers helped to improve the manuscript.

## References

Arnaud, N. O., Vidal, P., Tapponnier, P., Matte, P., & Deng, W. M. (1992). The high $K_2O$ volcanism of northwestern Tibet: Geochemistry and tectonic implications. *Earth and Planetary Science Letters*, *111*, 351–367.

Burchfiel, B. C., & Royden, L. H. (1985). North-south extension within the convergent Himalayan region. *Geology*, *13*, 679–682.

Chapman, J. B., Ducea, M. N., Kapp, P., Gehrels, G. E., & DeCelles, P. G. (2017). Spatial and temporal radiogenic isotopic trends of magmatism in Cordilleran orogens. *Gondwana Research*, *48*, 189–204.

Chemenda, A. I., Burg, J. P., & Mattauer, M. (2000). Evolutionary model of the Himalaya–Tibet system: Geopoem based on new modelling, geological and geophysical data. *Earth and Planetary Science Letters*, *174*, 397–409.

Chung, S. L., Chu, M. F., Ji, J., O'reilly, S. Y., Pearson, N. J., Liu, D., . . . Lo, C. H. (2009). The nature and timing of crustal thickening in Southern Tibet: Geochemical and zircon Hf isotopic constraints from postcollisional adakites. *Tectonophysics*, *477*, 36–48.

Chung, S. L., Liu, D., Ji, J., Chu, M. F., Lee, H. Y., Wen, D. J., . . . Zhang, Q. (2003). Adakites from continental collision zones: Melting of thickened lower crust beneath southern Tibet. *Geology*, *31*, 1021–1024.

DeCelles, P. G., Ducea, M. N., Kapp, P., & Zandt, G. (2009). Cyclicity in Cordilleran orogenic systems. *Nature Geoscience*, *2*, 251–257.

DeCelles, P. G., Kapp, P., Quade, J., & Gehrels, G. E. (2011). Oligocene–Miocene Kailas basin, southwestern Tibet: Record of postcollisional upper-plate extension in the Indus-Yarlung suture zone. *Geological Society of America Bulletin*, *123*, 1337–1362.

DeCelles, P. G., Robinson, D. M., & Zandt, G. (2002). Implications of shortening in the Himalayan fold-thrust belt for uplift of the Tibetan Plateau. *Tectonics*, *21*(6), 1062. https://doi.org/10.1029/2001TC001322

Deng, W. M. (1989). Cenozoic volcanic rocks in the northern Ngari district of the Tibet (Xizang), Discussion on the concurrent intracontinental subduction. *Acta Petrologica Sinica*, *3*.

Dewey, J. F., Shackleton, R. M., Chengfa, C., & Yiyin, S. (1988). The tectonic evolution of the Tibetan Plateau. *Philosophical Transactions of the Royal Society of London A: Mathematical and Physical Sciences*, *327*, 379–413.

Ding, L., Kapp, P., Zhong, D., & Deng, W. (2003). Cenozoic volcanism in Tibet: Evidence for a transition from oceanic to continental subduction. *Journal of Petrology*, *44*, 1833–1865.

Ducea, M. N., Paterson, S. R., & DeCelles, P. G. (2015). High-volume magmatic events in subduction systems. *Elements*, *11*, 99–104.

Faure, G., & Mensing, T. M. (2005). *Isotopes: Principles and applications* (928 p.). Hoboken, NJ: John Wiley.

Grujic, D., Hollister, L. S., & Parrish, R. R. (2002). Himalayan metamorphic sequence as an orogenic channel: Insight from Bhutan. *Earth and Planetary Science Letters*, *198*, 177–191.

Harrison, T. M., Copeland, P., Kidd, W. S. F., & Yin, A. N. (1992). Raising Tibet. *Science*, *255*, 1663–1670.

Hou, Z. Q., Zheng, Y. C., Zeng, L. S., Gao, L. E., Huang, K. X., Li, W., . . . Sun, Q. Z. (2012). Eocene–Oligocene granitoids in southern Tibet: Constraints on crustal anatexis and tectonic evolution of the Himalayan orogen. *Earth and Planetary Science Letters*, *349*, 38–52.

Ji, W. Q., Wu, F. Y., Chung, S. L., Li, J. X., & Liu, C. Z. (2009). Zircon U–Pb geochronology and Hf isotopic constraints on petrogenesis of the Gangdese batholith, southern Tibet. *Chemical Geology*, *262*, 229–245.

Kapp, P., DeCelles, P. G., Leier, A. L., Fabijanic, J. M., He, S., Pullen, A., . . . Ding, L. (2007). The Gangdese retroarc thrust belt revealed. *GSA Today*, *17*, 4–9.

Kapp, P., & Guynn, J. H. (2004). Indian punch rifts Tibet. *Geology*, *32*, 993–996.

Kelly, S., Butler, J. P., & Beaumont, C. (2016). Continental collision with a sandwiched accreted terrane: Insights into Himalayan–Tibetan lithospheric mantle tectonics? *Earth and Planetary Science Letters*, *455*, 176–195.

Kinny, P. D., & Maas, R. (2003). Lu–Hf and Sm–Nd isotope systems in zircon. *Reviews in Mineralogy and Geochemistry*, *53*, 327–341.

Lee, H. Y., Chung, S. L., Lo, C. H., Ji, J., Lee, T. Y., Qian, Q., & Zhang, Q. (2009). Eocene Neotethyan slab breakoff in southern Tibet inferred from the Linzizong volcanic record. *Tectonophysics*, *477*, 20–35.

Lee, J., & Whitehouse, M. J. (2007). Onset of mid-crustal extensional flow in southern Tibet: Evidence from U/Pb zircon ages. *Geology*, *35*, 45–48.

Mamani, M., Wörner, G., & Sempere, T. (2010). Geochemical variations in igneous rocks of the Central Andean orocline (13 S to 18 S): Tracing crustal thickening and magma generation through time and space. *Geological Society of America Bulletin*, *122*, 162–182.

McDonough, W. F., & Sun, S. S. (1995). The composition of the Earth. *Chemical Geology*, *120*, 223–253.

Owens, T. J., & Zandt, G. (1997). Implications of crustal property variations for models of Tibetan plateau evolution. *Nature*, *387*, 37–42.

Platt, J., & England, P. (1994). Convective removal of lithosphere beneath mountain belts-Thermal and mechanical consequences. *American Journal of Science*, *294*, 307–336.

Powell, C. M. (1986). Continental underplating model for the rise of the Tibetan Plateau. *Earth and Planetary Science Letters*, *81*, 79–94.

Replumaz, A., Negredo, A. M., Guillot, S., & Villaseñor, A. (2010). Multiple episodes of continental subduction during India/Asia convergence: Insight from seismic tomography and tectonic reconstruction. *Tectonophysics*, *483*, 125–134.

Roger, F., Tapponnier, P., Arnaud, N., SchaÈrer, U., Brunel, M., Zhiqin, X., & Jingsui, Y. (2000). An Eocene magmatic belt across central Tibet: Mantle subduction triggered by the Indian collision? *Terra Nova*, *12*, 102–108.

Royden, L. H., Burchfiel, B. C., King, R. W., Wang, E., Chen, Z., Shen, F., & Liu, Y. (1997). Surface deformation and lower crustal flow in eastern Tibet. *Science*, *276*, 788–790.

Sundell, K. E., Taylor, M. H., Styron, R. H., Stockli, D. F., Kapp, P., Hager, C., . . . Ding, L. (2013). Evidence for constriction and Pliocene acceleration of east-west extension in the North Lunggar rift region of west central Tibet. *Tectonics*, *32*, 1454–1479.

Tapponnier, P., Zhiqin, X., Roger, F., Meyer, B., Arnaud, N., Wittlinger, G., & Jingsui, Y. (2001). Oblique stepwise rise and growth of the Tibet Plateau. *Science*, *294*, 1671–1677.

Turner, S., Arnaud, N., Liu, J., Rogers, N., Hawkesworth, C., Harris, N., . . . Deng, W. (1996). Post-collision, shoshonitic volcanism on the Tibetan Plateau: Implications for convective thinning of the lithosphere and the source of ocean island basalts. *Journal of Petrology*, *37*, 45–71.

Turner, S., Hawkesworth, C., Liu, J., Rogers, N., Kelley, S., & van Calsteren, P. (1993). Timing of Tibetan uplift constrained by analysis of volcanic rocks. *Nature*, *364*, 50–54.

Vervoort, J. D., Patchett, P. J., Blichert-Toft, J., & Albarède, F. (1999). Relationships between Lu–Hf and Sm–Nd isotopic systems in the global sedimentary system. *Earth and Planetary Science Letters*, *168*, 79–99.

Wang, J. H., Yin, A., Harrison, T. M., Grove, M., Zhang, Y. Q., & Xie, G. H. (2001). A tectonic model for Cenozoic igneous activities in the eastern Indo–Asian collision zone. *Earth and Planetary Science Letters*, *188*, 123–133.

Wang, Q., McDermott, F., Xu, J. F., Bellon, H., & Zhu, Y. T. (2005). Cenozoic K-rich adakitic volcanic rocks in the Hohxil area, northern Tibet: Lower-crustal melting in an intracontinental setting. *Geology*, *33*, 465–468.

Xu, Y. G., Lan, J. B., Yang, Q. J., Huang, X. L., & Qiu, H. N. (2008). Eocene break-off of the Neo-Tethyan slab as inferred from intraplate-type mafic dykes in the Gaoligong orogenic belt, eastern Tibet. *Chemical Geology*, *255*, 439–453.

Yin, A. (2006). Cenozoic tectonic evolution of the Himalayan orogen as constrained by along-strike variation of structural geometry, exhumation history, and foreland sedimentation. *Earth-Science Reviews*, *76*, 1–131.

Yin, A. (2010). Cenozoic tectonic evolution of Asia: A preliminary synthesis. *Tectonophysics*, *488*, 293–325.

Yin, A., & Harrison, T. M. (2000). Geologic evolution of the Himalayan-Tibetan orogen. *Annual Review of Earth and Planetary Sciences*, *28*, 211–280.

Yin, A., Harrison, T. M., Ryerson, F. J., Wenji, C., Kidd, W. S. F., & Copeland, P. (1994). Tertiary structural evolution of the Gangdese thrust system, southeastern Tibet. *Journal of Geophysical Research*, *99*, 18175–18201.

Zhang, Z., Zhao, G., Santosh, M., Wang, J., Dong, X., & Shen, K. (2010). Late Cretaceous charnockite with adakitic affinities from the Gangdese batholith, southeastern Tibet: Evidence for Neo-Tethyan mid-ocean ridge subduction? *Gondwana Research*, *17*, 615–631.

Zhu, D. C., Zhao, Z. D., Niu, Y., Mo, X. X., Chung, S. L., Hou, Z. Q., . . . Wu, F. Y. (2011). The Lhasa Terrane: Record of a microcontinent and its histories of drift and growth. *Earth and Planetary Science Letters*, *301*, 241–255.